



Reaction kinetics of bond rotations in graphene



Stephen T. Skowron^a, Victor O. Koroteev^{b, c}, Matteo Baldoni^a, Sergei Lopatin^d,
Amaia Zurutuza^e, Andrey Chuvilin^{f, g, **}, Elena Besley^{a, *}

^a School of Chemistry, University of Nottingham, University Park, Nottingham, NG7 2RD, UK

^b Nikolaev Institute of Inorganic Chemistry, SB RAS, Lavrentiev ave. 3, 630090, Novosibirsk, Russia

^c Novosibirsk State University, Pirogova st. 2, 630090, Novosibirsk, Russia

^d King Abdulla University of Science & Technology, Thuwal, Makkah, 23955, Saudi Arabia

^e Graphenea S.A., Tolosa Hiribidea 76, 20018, Donostia-San Sebastián, Spain

^f CIC nanoGUNE Consolider, Av. de Tolosa 76, E-20018, Donostia-San Sebastian, Spain

^g IKERBASQUE Basque Foundation for Science, E-48013, Bilbao, Spain

ARTICLE INFO

Article history:

Received 29 February 2016

Received in revised form

5 April 2016

Accepted 10 April 2016

Available online 12 April 2016

ABSTRACT

The formation and healing processes of the fundamental topological defect in graphitic materials, the Stone-Wales (SW) defect, are brought into a chemical context by considering the rotation of a carbon–carbon bond as chemical reaction. We investigate the rates and mechanisms of these SW transformations in graphene at the atomic scale using transmission electron microscopy. We develop a statistical atomic kinetics formalism, using direct observations obtained under different conditions to determine key kinetic parameters of the reactions. Based on the obtained statistics we quantify thermally and irradiation induced routes, identifying a thermal process of healing with an activation energy consistent with predicted adatom catalysed mechanisms. We discover exceptionally high rates for irradiation induced SW healing, incompatible with the previously assumed mechanism of direct knock-on damage and indicating the presence of an efficient nonadiabatic coupling healing mechanism involving beam induced electronic excitations of the SW defect.

Crown Copyright © 2016 Published by Elsevier Ltd. All rights reserved.

1. Introduction

The emergence of low-voltage, aberration-corrected, high-resolution transmission electron microscopy (AC-HRTEM) with high spatial and temporal resolution has made *in situ* monitoring of dynamic processes in graphitic nanomaterials at a single-atom level routinely accessible [1–3]. Observations of the dynamic behaviour of extended atomic-scale lattice defects [4,5] and the transformation of carbon nanostructures under the electron beam (e-beam) [6,7], in some cases leading to the formation of entirely new nanostructures [8,9], have attracted considerable interest. Our recent review [10] discusses the energetics of these processes, detailing the wide variety of thermally and irradiation induced structure changes in graphene. Analysing AC-HRTEM image

sequences of elementary steps of structure change can facilitate an understanding of the overall reaction and provide information about the reaction mechanism [8]. However, quantitative experimental assessment of the kinetics of single defect transformations is perceived to be extremely difficult. Important chemical and kinetic parameters of the elementary atomic rearrangements can be, in principle, extracted from a rigorous statistical treatment of a large number of directly observed events [11]. In this approach, the high-energy electrons of the imaging beam also serve as a source of energy to initiate the chemical reaction, similar to the effect of high temperature.

Electron beam induced reactions are typically described in terms of the reaction cross-section, which depends on the energy of the incident beam and the minimum threshold energy required to activate the reaction [12]. The reaction cross-section defines the probability of a single reaction for a given flux of incident electrons, and determines the relative rates of such processes. The *irreversible* process of atom emission is the most significant and potent e-beam induced structure modification, and the cross-section of this process in graphene has been derived experimentally [11,13]. This

* Corresponding author.

** Corresponding author. CIC nanoGUNE Consolider, Av. de Tolosa 76, E-20018, Donostia-San Sebastian, Spain.

E-mail addresses: achuvilin@nanogune.eu (A. Chuvilin), elena.besley@nottingham.ac.uk (E. Besley).

cross-section is also well known theoretically in both graphene [14] and other carbon nanomaterials such as nanotubes [15,16], graphene flakes [17], and graphene nanoribbons [18]. The other major transformation - the rotation of a single carbon-carbon bond by 90° leading to the Stone-Wales (SW) defect [19] - is, unlike atom emission, a *directly reversible* process. The SW defect is a fundamentally important topological defect, and the SW transformation underpins a wide variety of dynamical behaviour in graphene [20]. Its easily reversible nature makes experimental estimation of the cross-sections a formidable task. The threshold energies of SW transformations have only been estimated theoretically, and cross-sections have not been predicted even computationally due to the complex anisotropy of these threshold energies [20,21]. Meanwhile, the equivalent kinetic parameters for the thermally activated reactions have been widely studied theoretically; but despite this extensive interest and key relevance to the targeted structural modification of graphene, experimental kinetics studies have thus far remained inaccessible.

In this paper, we develop a statistical atomic kinetics formalism for measurements of reaction rates and apply it to study bond rotations (SW transformations) in graphene. We use the e-beam to activate the reaction, and apply a rigorous statistical treatment of individual SW transformations, directly observed at atomic resolution by AC-HRTEM, to decouple the key processes contributing to the reaction. This separation of thermal and e-beam induced routes allows us to fully characterise the kinetic parameters of each mechanism, providing the first experimentally derived values for the irradiation cross-sections and thermal activation energies of SW transformations in graphene. Finally, a comparison of these values with theoretical predictions provides intriguing mechanistic insight into the underlying atomic processes.

2. Rate constants and cross-sections of reversible beam induced reactions

In this section, atomistic beam induced reactions are considered in analogy to macroscopic reaction kinetics. An approach is developed by which macroscopic rate constants and reaction cross-sections can be extracted from the statistics of many atomic-scale observations in TEM.

In the framework of chemical kinetics the rate of a unimolecular reaction, in which species *A* simply rearranges itself to produce one or more products, is generally given as

$$-\frac{d[A]}{dt} = k[A] \quad (1)$$

where *k* is the reaction rate constant. For a thermally induced reaction, the temperature dependence of the thermal reaction rate constant *k^t* is often given by the Arrhenius equation

$$k^t = P \cdot \exp\left(\frac{-E_a}{k_B T}\right) \quad (2)$$

P is the frequency factor (the rate of particle collisions in gas or liquid, or the rate of bond vibrations in a solid), while the exponent is the probability factor or the success rate of the considered process, namely the proportion of particles at temperature *T* with a greater energy than the activation energy *E_a*. The rate of an equivalent irradiation induced reaction can be expressed as

$$-\frac{d[A]}{dt} = j\sigma[A] \quad (3)$$

j is the irradiation flux (in nm⁻² s⁻¹) and *σ* is the reaction cross-

section, which has a dimension of area (1 b = 10⁻¹⁰ nm²). The macroscopic rate constant of the irradiation induced reaction *kⁱ* can be defined as

$$k^i = j\sigma \quad (4)$$

In relation to the Arrhenius Eq. (2), for an irradiation induced reaction the frequency factor is now expressed as the irradiation flux *j*, while the probability factor is simply the reaction cross-section *σ*. It should be stressed that the kinetic analysis presented here makes no assumptions regarding the mechanism of the beam induced reaction (or, indeed, of the nature of the beam) and so the cross-sections measured using this approach and presented in this paper are similarly independent of any particular mechanism. Mechanistic insight can be obtained by comparing these cross-sections to theoretically calculated ones corresponding to a particular process, as we discuss later.

The direct relationship (4) between the reaction rate constant defined macroscopically and the atomistic value of the reaction cross-section, in principle, allows experimental techniques traditionally used to obtain one to be used to acquire the other. Many decades of progress in physical chemistry can be exploited to guide the transition of reaction kinetics techniques into the emerging field of nanoscience, in which the concept of cross-sections of key processes has been essential for understanding nanostructure transformations under external influences. Recent developments in atomic-scale imaging techniques enable observations of single atoms taking part in a reaction; this potentially allows the calculation of reaction rate constants *directly*, in a bottom-up approach. Chemical kinetics studies based on the direct observation of atom rearrangements can provide invaluable insight into the elementary steps of reaction and reaction routes, which are inaccessible to macroscopic chemical methods.

This concept is particularly well suited for studying the formation and transformations of atomic-scale defects in monolayer graphene. For *irreversible* e-beam induced processes, such as atom ejection, the reaction rate constant of defect formation can be obtained simply from the accumulation of the product with time [11], directly from Eq. (3). The reaction rate of a *reversible* reaction, e.g. the formation and healing of defect species *D* under the e-beam, is determined by the rate of both defect formation and defect healing, denoted by subscripts *f* and *h*, respectively

$$\frac{d[D]}{dt} = k_f([C]_0 - [D]) - k_h[D] \quad (5)$$

[*C*]₀ is the density of atoms in the pristine sample, which in the case of graphene is defined per unit area (not per unit volume). Classical chemical kinetics observes the macroscopic outcome of *both* reactions, i.e. the change in the concentration of species *D*, while AC-HRTEM enables the direct observation of each reaction *individually*. Eq. (5) can be split into two independent equations, similar to (3), the left side of which denote the number of formation events *n_f*, or healing events *n_h*, per unit time per unit area, rather than the change in concentration:

$$\frac{n_f}{dt} = k_f^i([C]_0 - [D]) = j\sigma_f([C]_0 - [D]) \quad (6)$$

$$\frac{n_h}{dt} = k_h^i[D] = j\sigma_h[D] \quad (7)$$

As the healing rate depends on the defect concentration [*D*], which is very low and difficult to measure exactly, it is convenient to consider the healing of defects on an individual basis using the finite difference form of Eq. (7) setting [*D*] and *n_h* to 1 nm⁻².

$$\frac{1}{\langle Dt \rangle} = k_h^i = j\sigma_h \quad (8)$$

Eq. (8) reformulates the problem in terms of the average lifetime Dt of a single defect, rather than the aggregate reaction rate, thus removing the dependence on the defect concentration and allowing for the direct measurement of the healing rate from the experimental image series. The average lifedose (the dose of electrons required to heal the defect) is related to the average lifetime as

$$\langle X \rangle = \langle Dt \rangle j = \frac{1}{\sigma_h} \quad (9)$$

Note from Eq. (9) that for the irradiation induced first order reaction the lifedose does not depend on the electron flux, which will become important in the discussion of the results.

In the case of reversible processes, such as SW transformations, there is an additional complication related to the fact that the lifetime of a defect can be very short, so that its creation and subsequent elimination passes unnoticed by the image recording system. The principal limitation for temporal resolution in AC-HRTEM is the shot noise, which we have discussed in detail previously [17]. The visibility (an obtainable signal-to-noise ratio) of a particular atomic configuration is defined by the relation between the lifedose and the minimum electron dose required to image it. The other limitation for temporal resolution is the speed of the imaging device, which in our case corresponds to a minimum frame time of 50 ms. In order to understand the visibility of the SW transformations in detail we have performed extensive image simulations, accounting for the lifetime of the defect, shot noise and modulation function of the CCD camera. Details can be found in the [Supporting Information](#). These simulations show that the minimum electron dose required to identify the SW defect (the shot noise limit) is $\sim 10^5 \text{ nm}^{-2}$; and in the case of a high signal-to-noise ratio the SW defect is recognisable in the image once it has lived more than 10% of the frame time.

The inaccessibility of the short-lived defects leads to an over-estimation of the average lifedose and consequently to an under-estimation of the healing cross-section, σ_h , derived from Eq. (9). A solution to this problem can be found if we note that the actual value of the lifedose is statistically distributed due to the stochastic nature of the process. The probability distribution of the lifedose X follows the geometric distribution (see the [Supporting Information](#)

for further discussion, note that σ_h and X are dimensionless here):

$$Q(X) = \frac{n_h(X)}{N} = (1 - \sigma_h)^{X-1} \sigma_h \quad (10)$$

where $n_h(X)$ is the experimentally observed number of healing events happened after deposition of dose X , and N is a total number of created defects including invisible short-lived ones. Although the lower part of this distribution is missed due to the limited temporal resolution, it still can be fitted to experimental data, with σ_h and N as free parameters. This provides an unbiased measure of σ_h independent of the one obtained from Eq. (9). At the same time an unbiased value for σ_f accounting for the short-lived defects can be calculated using N and Eq. (6).

3. Experimental results

We begin this section by examining SW defect formation, experimentally quantifying the rates of thermally and irradiation induced pathways, and then accounting for short-lived defects. This is followed by a similar treatment for the process of SW defect healing. These results are then summarised and compared to theoretical expectations. In the discussion we consider the very large discrepancies between existing theory and this experimental data, and propose a potential explanation for the observed cross-sections.

SW defect transformations were induced and imaged using AC-HRTEM, in areas of pristine graphene $100\text{--}200 \text{ nm}^2$ in size. Fourteen series of images at a 60 keV beam energy and nine series of images at 80 keV were recorded at a variety of electron fluxes ranging from 6.8×10^5 to $2.1 \times 10^7 \text{ nm}^{-2} \text{ s}^{-1}$. AC-HRTEM images were recorded continuously at 10 frames per second, and over 10,000 frames were analysed. In each image series lasting 20–50 s, zero to twenty-four SW defects were observed, typically lasting from 0.1 s to 1 s. In total, 114 SW defects were recorded at 60 keV, and 68 SW defects were recorded at 80 keV. The obtained images have been processed to simplify the detection of SW defects (see the [Supporting Information](#) for details of imaging and processing). Fig. 1 shows a typical example of a single defect and Supporting Video 1 shows one of the experimental series with the defects indicated.

Supplementary data related to this article can be found online at <http://dx.doi.org/10.1016/j.carbon.2016.04.020>.

The cross-section of SW formation, σ_f , can be estimated from Eq. (6) in two independent ways: in the integral form as a total number

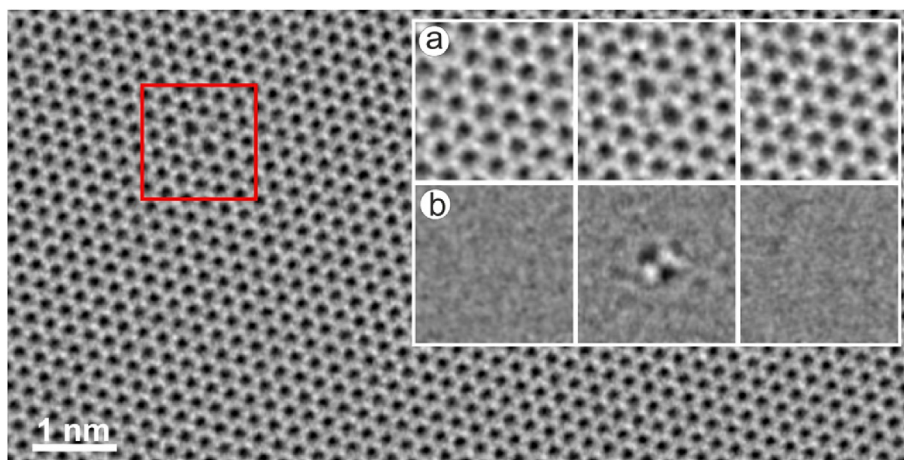


Fig. 1. Example image of a SW defect in pristine graphene from an image series at 80 keV. Inset shows area bordered in red: (a) example sequence of a SW defect forming and then healing to return to pristine graphene over 3 s (1 s per image); (b) the same images with the graphene lattice removed by Fourier filtering, showing the characteristic 'dumbbell' signal of a SW defect. (A colour version of this figure can be viewed online.)

of observed formation events per total area per total dose, and as the slope of a linear plot showing the SW formation rate as a function of electron flux (see Fig. 2). We assume that the concentration of SW defects $[D]$ is negligible compared to the area density of carbon atoms in graphene ($[C]_0 = 38.2 \text{ nm}^{-2}$, see the Supporting Information for discussion concerning low $[D]$). These two estimations give the respective values for the σ_f of (0.059 ± 0.006) and (0.067 ± 0.017) barn for 60 keV, and (0.066 ± 0.008) and (0.060 ± 0.008) barn for 80 keV. It is important to note that, within the reported error bars, the values for the σ_f obtained by two independent methods are intrinsically the same. As short-lived SW defects were not captured by AC-HRTEM, these cross-sections can only be considered as reliable estimates for the lower limit.

An excellent agreement between the values measured by the integral approach and as a coefficient of linear regression not only demonstrates the consistency of the obtained data and interpretation, but also indicates that there is no significant contribution from non-irradiative, i.e. thermal, reaction pathways. In particular, this is evident from the y -intercept of fitted straight lines in Fig. 2 being statistically consistent with zero for both beam energies. In the presence of a thermal pathway and assuming $[D] \ll [C]_0$ Eq. (6) becomes

$$\frac{n_f}{dt} = (j\sigma_f + k_h^t)[C]_0 \quad (11)$$

where k_h^t is the thermal reaction rate constant of SW formation. Assuming that the thermally induced formation rate does not depend on the e-beam energy, from the two intercepts we obtain the average estimate of $k_h^t = (0.3 \cdot 10^{-6} \pm 1.1 \cdot 10^{-5}) \text{ s}^{-1}$. Taking the upper limit for k_h^t defined by the error bar as $1.41 \cdot 10^{-5} \text{ s}^{-1}$, assuming the frequency pre-factor P in Eq. (2) of the order of 10^{12} s^{-1} (computed for the SW defect in graphene [22]) and the temperature of the sample as 300 K, we obtain a lower estimate for the activation energy of thermally induced formation of SW defects as $E_f = 23 \text{ kcal/mol}$ (or 1.0 eV).

In order to account for short-lived and thus undetected defects we have measured the lifedose of each of the 182 observed SW defects, and fitted their distribution to the geometric distribution (10) as shown in Fig. 3 (details are in the Supporting Information). The total number of created SW defects was calculated to be 186 at

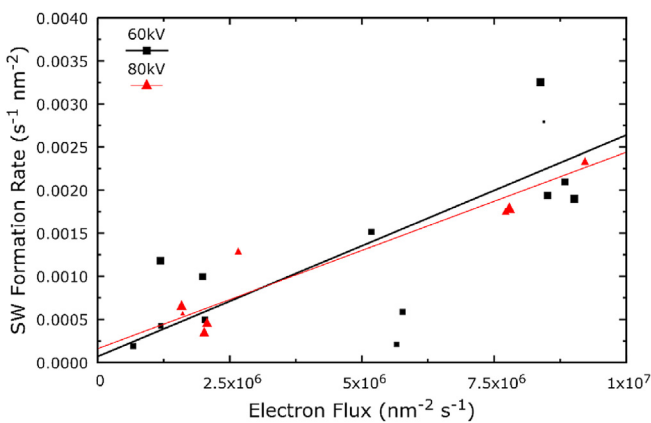


Fig. 2. The formation rate of SW defects as a function of electron flux at 60 keV (black squares) and 80 keV (red triangles). Weighted least-square regressions are given by the black and thin red lines respectively. The size of each point is proportional to the product of the area and time for corresponding image series, which is used for the weighting of the fitting. Values of the intercept with the y -axis were calculated to be $(6.73 \times 10^{-5} \pm 3.94 \times 10^{-4}) \text{ s}^{-1} \text{ nm}^{-2}$ for 60 keV and $(1.59 \times 10^{-4} \pm 1.60 \times 10^{-4}) \text{ s}^{-1} \text{ nm}^{-2}$ for 80 keV. (A colour version of this figure can be viewed online.)

60 keV and 169 at 80 keV; using these estimated totals, the revised values of the formation cross-sections, σ_f , are (0.096 ± 0.004) barn at 60 keV and (0.164 ± 0.013) barn at 80 keV, with the standard errors associated with the geometric distribution fitting.

Estimation of the thermal contribution in the case of healing with a method similar to that used for formation is problematic, as the healing rate is difficult to measure in terms of concentration; as discussed, $[D]$ is very low. Hence, we will use the lifetime formalism as an alternative approach. In the presence of a thermally induced co-reaction, Eq. (8) becomes

$$\frac{1}{\langle Dt \rangle} = j\sigma_h + k_h^t \quad (12)$$

where k_h^t is the rate constant for thermally induced healing of a SW defect. Plotting the data in $(\frac{1}{\langle Dt \rangle}; j)$ coordinates (Fig. 4), we obtain σ_h as a slope of the best fit, and k_h^t as the y -intercept. Although Figs. 2 and 4 look very similar, we should emphasise that their physical meaning is substantially different. The y -intercepts of the straight lines shown in Fig. 4 are significantly (in the statistical sense) non-zero for both 60 and 80 keV beam energies, although might be considered equal within the error bars. The average value for k_h^t is estimated as $(0.56 \pm 0.53) \text{ s}^{-1}$. Making the same assumptions as for the SW formation process, the activation energy for thermally induced healing is $E_h = 16.8_{-0.4}^{+1.7} \text{ kcal/mol}$ (or $0.73_{-0.02}^{+0.07} \text{ eV}$). The cross-section for the irradiation induced reaction estimated from the slope is (3400 ± 500) barn at 60 keV and (3000 ± 200) barn at 80 keV. As in the case of SW formation, these

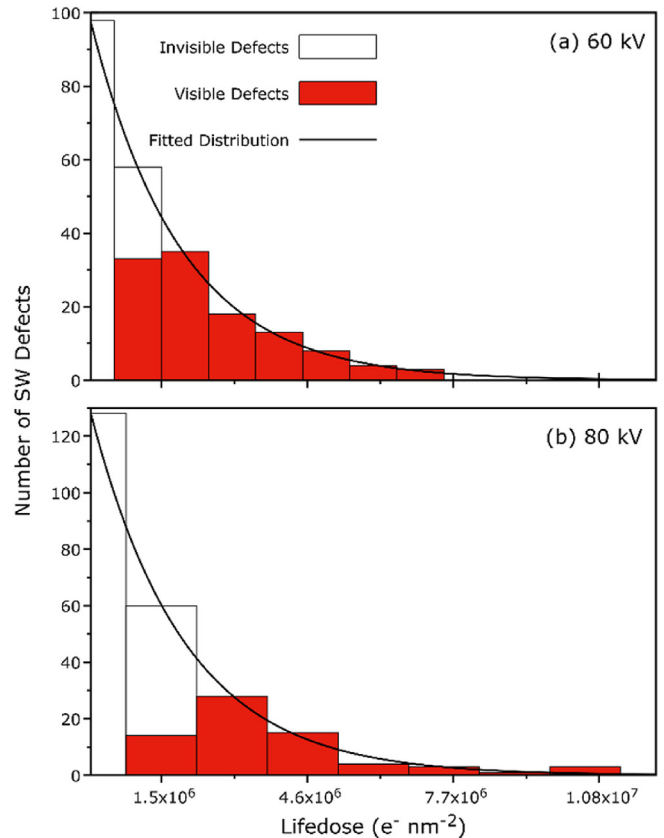


Fig. 3. The number of SW defects with a lifedose falling in each bin (red bars) and the geometric distribution (10) fitted to the experimental data at (a) 60 keV and (b) 80 keV (black lines). The white bars at lower doses show the projected number of undetected SW defects obtained from the geometric distribution (10). (A colour version of this figure can be viewed online.)

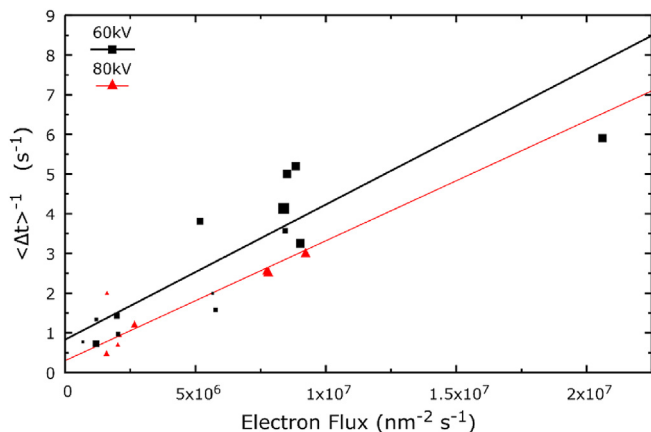


Fig. 4. Inverse of the average healing time as a function of electron flux for each series of images at 60 keV (black squares) and 80 keV (red triangles). The weighted linear regression of the experimental data is shown by the black and thin red lines, respectively. The size of each point is proportional to the number of SW defects, used for the weighting of the fitting. The obtained slopes are 60 keV: $(3.4 \times 10^{-7} \pm 0.5 \times 10^{-7}) \text{ nm}^2$ (3400 b) and 80 keV: $(3.0 \times 10^{-7} \pm 0.2 \times 10^{-7}) \text{ nm}^2$ (3000 b), and the intercepts are 60 keV: $(0.83 \pm 0.51) \text{ s}^{-1}$ and 80 keV $(0.30 \pm 0.13) \text{ s}^{-1}$. (A colour version of this figure can be viewed online.)

cross-sections should be taken as reliable lower estimates due to the presence of unobserved short-lived defects. Better statistics have the potential for a substantial improvement of the reliability of these values; for this, the number of events required would need to be suitable for fitting distribution (10) at each electron flux.

At this point, we should comment on the relevance of the statistical fit shown in Fig. 3, which did not account for the thermal contribution to the healing process. Thermally induced events should follow the same statistics as radiation induced ones if the underlying physical process of energy transfer via sequential collisions is the same. However, the number of thermally activated events should be sampled over the lifetime rather than the lifedose. Although the latter is not a direct function of the former (due to the use of different electron fluxes in the different experimental series) they are correlated: at any fixed flux there is a linear relation between the two. This implies that the shape of the distribution will not be dramatically affected and thus the total number of events can be estimated accurately. Of course the meaning of σ_h determined from this distribution becomes obsolete; however the total number of the existed defects N remains accurate, as do the values for formation cross-section, σ_f , derived from it.

4. Discussion

Table 1 summarises the obtained values of cross-sections and activation energies in comparison to theoretical predictions found

Table 1
Summary of our measured cross-sections of irradiation induced processes and activation energies of thermally induced processes (in bold), in comparison with theoretical estimations from the literature (in italics). Cross-sections are given per atom for formation and per defect for healing.

		60 keV	80 keV
SW formation	Irradiation induced, σ_f	0.096 \pm 0.004 b <i>Upper limit: 0.0006 b^a</i> <i>Lower limit: 1.0 eV</i>	0.164 \pm 0.013 b <i>Upper limit: 0.302 b^a</i>
	Thermal, E_f	8–9 eV [25,27], <i>adatom catalysis: 2.3 eV [25]</i>	
SW healing	Irradiation induced, σ_h	3400 \pm 500 b <i>Upper limit: 5.8 b^a</i>	Lower limit: 3000 \pm 200 b <i>Upper limit: 37.0 b^a</i>
	Thermal, E_h	0.73 ^{+0.07} _{-0.02} eV 3.4–6.2 eV [25–27], <i>adatom catalysis: 0.7–0.87 eV [25,26]</i>	

^a Theoretical upper limits for cross-sections calculated assuming processes of direct knock-on damage, using the McKinley-Feshbach approximation [24] - isotropic approximations of the threshold energies of 19 and 13 eV [21] for formation and healing provide upper limits of the true anisotropic cross-sections.

in the literature. It is important to note that all existing works describing the SW transformation under electron irradiation have considered solely ballistic atom displacements (direct knock-on damage) [4,20,21,23], which is well described by the McKinley-Feshbach approximation [18,24]; in contrast the cross-sections measured in this work do not include any assumptions about the mechanism of energy transfer from the electron beam to the sample. As is seen in Table 1, only a few values fit well to theoretical expectations: the lower limit of thermal activation energy for formation is indeed lower than any theoretical estimation; the thermal activation energy for healing is much lower than theoretical values for direct healing, however it corresponds well to a predicted [25,26] adatom catalysed mechanism; σ_f at 80 keV is slightly below the predicted upper limit. The rest of the results are in striking disagreement to theoretical expectations. If the theoretical estimation for σ_f was correct for 60 keV, not a single SW defect would be observed at this beam energy throughout the duration of all our experimental series, while we see them appearing at a similar rate as at 80 keV. The observed σ_f exceeds the theoretical value by 3 orders of magnitude.

Similarly, the experimentally measured cross-sections for healing at both beam energies are dramatically higher than expected for the ballistic mechanism. Theoretical values of σ_h (based on this mechanism of direct knock-on damage, with a threshold energy calculated as 13 eV [21]) imply that the lifetime of a SW defect should be of the order of 100 s in our conditions, which is very different to what we (and others [20]) observe experimentally. Both σ_h values measured for 60 and 80 keV are consistent with a knock-on threshold energy of approximately 0.56 eV, as would be determined from the McKinley-Feshbach formula [24]. This value is inconsistent in two ways: first, it is significantly (in the statistical sense) *smaller* than the measured E_h , which is physically impossible (see Supporting Information for discussion); and secondly, if a reaction pathway with $E_h < 0.56$ eV existed, it would result in a characteristic thermal healing time of less than 0.01 s, in which case SW defects would be undetectable in our experiments. As the McKinley-Feshbach formula describes direct electron-nucleus collisions, the above contradictions unambiguously rule out, for the considered reactions, such collisions as the only mechanism of energy transfer from electron beam to atomic nuclei in graphene. This also includes any potential catalytic pathways allowing energy supply via multiple electron collisions, suggested earlier as an explanation for unexpectedly high reaction rates in bi-layer graphene [28]. If such a catalytic route existed, it would be more efficiently realised thermally rather than under irradiation, as discussed above.

One potential explanation for the high reaction rates could be heating induced by the electron beam. Although the average temperature increase in the electron beam is estimated not to be higher than 1 K [29,30], every electron colliding with the lattice atoms

creates a thermalized spot in which the temperature may be very high. As the size of such spots is substantially larger than the size of SW defect, the reaction might potentially be activated by electron-to-nucleus collisions in an extended area, thus effectively increasing the cross-section. We have thoroughly investigated (see the [Supporting Information](#)) the effect of such thermal spikes on the reaction rate and concluded that, for our experimental conditions, thermal spikes are too short-lived to have any substantial contribution.

As electron-nucleus interactions have been eliminated as a possible mechanism leading to quick healing of the SW defect, we now consider routes of energy transfer via excitation of the electron system of graphene. The typical cross-sections for emission of core electrons are of the order of thousands barn (as an example, Egerton [12] estimates the radiolysis cross-section of elemental carbon to be 2100 b at 100 keV). The high conductivity of graphene precludes ionisation as a mechanism of structural changes – quenching by conduction electrons will occur on a much quicker timescale than bond rotation. However, inter and intra band excitations of electrons in graphene have been determined to have anomalously long lifetimes in the order of 10 ps [31–33], and a conical intersection was shown to provide a nonadiabatic pathway for the SW rotation in a pyrene model, reducing the activation energy when starting from an electronically excited state [34]. The authors of this study speculate that “there should be nonnegligible effects of electronic excitation and nonadiabatic transitions (NATs) on the reaction mechanism of SWR induced by electron irradiation.”

A theoretical study of the response of the SW defect in graphene to ultrafast laser pulses [35] indicates that relaxation of excited electronic states occurs through the generation of strong localised transversal vibrations at the defect. The amplitude of the vibrations increases until a suitably high proportion of electrons are excited (6%, 1.3 eV absorbed per atom), above which the SW defect will spontaneously heal in only ~420 fs. In TEM, the electron beam can take the place of the laser pulses, electronically exciting the defect. As the cross-sections of low energy electron excitations by the electron beam in TEM may be exceptionally high (we measure about 2×10^7 b for 4.5 eV plasmon excitation in monolayer graphene) these interactions may result in a sufficient average population of excited states in order to cause spontaneous healing of the SW defect. The healing occurs via bond breaking with out-of-plane motion of the dimer, and consequent dimer rotation [35]. The localisation of coherent transversal phonon modes around lattice imperfections provides an explanation for the orders of magnitude faster backward bond rotation (SW healing) as compared to the direct rotation (SW formation). The lability of the rotated bond in more complex defects may be responsible for their high mobility under electron beam (see [Supporting Video 2](#) as an example) and in the future may serve as a means for engineering desired defective structures in graphene.

Supplementary data related to this article can be found online at <http://dx.doi.org/10.1016/j.carbon.2016.04.020>.

5. Conclusions

We have developed and tested a new statistical atomic kinetics approach for measuring kinetic parameters of chemical reactions. The proposed methodology has been validated and experimentally demonstrated using the fundamental reaction of bond rotation in graphene. The concept, however, is more general and can be extended to other reactions that can be accessed by AC-HRTEM. It has been shown that the proposed approach allows for the discrimination between irradiation induced and thermally activated reaction pathways; activation energies of elementary

reaction steps can be determined for the latter.

The obtained values for thermally activated reaction rates for SW formation and healing are in good agreement with theoretical predictions. However, the measured irradiation induced rates of healing exceed theoretical expectations by at least 3 orders of magnitude, ruling out the possibility of a mechanism mediated by direct knock-on damage. Instead, beam induced electronic excitation is likely to be the primary channel of SW defect healing, with the expected knock-on damage pathway negligible in comparison. As the SW transformation is an elementary step of defect conversion and migration in graphene, detailed knowledge of this process is vital to the understanding, controlling and engineering of defects in graphene.

Acknowledgements

E.B. acknowledges the ERC Consolidator grant (ERC-2012-StG 307755 FIN Grant). A.C. acknowledges a financial support from FEI Company (Netherlands) within a collaborative project. M. B. and E. B. are grateful to the High Performance Computing (HPC) Facility at the University of Nottingham for providing computational time. A.C. and V.K. acknowledge financial support via FP7-PEOPLE-2011-IRSES N295180 MagNonMag project.

Appendix A. Supplementary data

Supplementary data related to this article can be found at <http://dx.doi.org/10.1016/j.carbon.2016.04.020>.

References

- [1] A. Hashimoto, K. Suenaga, A. Gloter, K. Urita, S. Iijima, Direct evidence for atomic defects in graphene layers, *Nature* 430 (2004) 870–873, <http://dx.doi.org/10.1038/nature02817>.
- [2] K. Suenaga, H. Wakabayashi, M. Koshino, Y. Sato, K. Urita, S. Iijima, Imaging active topological defects in carbon nanotubes, *Nat. Nanotechnol.* 2 (2007) 358–360, <http://dx.doi.org/10.1038/nnano.2007.141>.
- [3] J.C. Meyer, A.K. Geim, M.I. Katsnelson, K.S. Novoselov, T.J. Booth, S. Roth, The structure of suspended graphene sheets, *Nature* 446 (2007) 60–63, <http://dx.doi.org/10.1038/nature05545>.
- [4] J. Kotakoski, A.V. Krasheninnikov, U. Kaiser, J.C. Meyer, From point defects in graphene to two-dimensional amorphous carbon, *Phys. Rev. Lett.* 106 (2011) 105505, <http://dx.doi.org/10.1103/PhysRevLett.106.105505>.
- [5] O. Lehtinen, S. Kurasch, A.V. Krasheninnikov, U. Kaiser, Atomic scale study of the life cycle of a dislocation in graphene from birth to annihilation, *Nat. Commun.* 4 (2013), <http://dx.doi.org/10.1038/ncomms3098>.
- [6] A. Chuvilin, J.C. Meyer, G. Algara-Siller, U. Kaiser, From graphene constrictions to single carbon chains, *New J. Phys.* 11 (2009) 083019, <http://dx.doi.org/10.1088/1367-2630/11/8/083019>.
- [7] C.O. Girit, J.C. Meyer, R. Erni, M.D. Rossell, C. Kisielowski, L. Yang, et al., Graphene at the edge: stability and dynamics, *Sci.* (80-) 323 (2009) 1705–1708, <http://dx.doi.org/10.1126/science.1166999>.
- [8] A. Chuvilin, U. Kaiser, E. Bichoutskaia, N.A. Besley, A.N. Khlobystov, Direct transformation of graphene to fullerene, *Nat. Chem.* 2 (2010) 450–453, <http://dx.doi.org/10.1038/nchem.644>.
- [9] A. Chuvilin, E. Bichoutskaia, M.C. Gimenez-Lopez, T.W. Chamberlain, G.A. Rance, N. Kuganathan, et al., Self-assembly of a sulphur-terminated graphene nanoribbon within a single-walled carbon nanotube, *Nat. Mater.* 10 (2011) 687–692, <http://dx.doi.org/10.1038/nmat3082>.
- [10] S.T. Skowron, I.V. Lebedeva, A.M. Popov, E. Bichoutskaia, Energetics of atomic scale structure changes in graphene, *Chem. Soc. Rev.* 44 (2015) 3143–3176, <http://dx.doi.org/10.1039/C4CS00499J>.
- [11] J.C. Meyer, F. Eder, S. Kurasch, V. Skakalova, J. Kotakoski, H.J. Park, et al., Accurate measurement of electron beam induced displacement cross sections for single-layer graphene, *Phys. Rev. Lett.* 108 (2012) 196102, <http://dx.doi.org/10.1103/PhysRevLett.108.196102>.
- [12] R.F. Egerton, Mechanisms of radiation damage in beam-sensitive specimens, for TEM accelerating voltages between 10 and 300 kV, *Microsc. Res. Tech.* 75 (2012) 1550–1556, <http://dx.doi.org/10.1002/jemt.22099>.
- [13] J.C. Meyer, F. Eder, S. Kurasch, V. Skakalova, J. Kotakoski, H.J. Park, et al., Erratum: accurate measurement of electron beam induced displacement cross sections for single-layer graphene [Phys. Rev. Lett. 108, 196102 (2012)], *Phys. Rev. Lett.* 110 (2013) 239902, <http://dx.doi.org/10.1103/PhysRevLett.110.239902>.
- [14] A. Zobelli, A. Gloter, C.P. Ewels, G. Seifert, C. Colliex, Electron knock-on cross

- section of carbon and boron nitride nanotubes, *Phys. Rev. B* 75 (2007) 245402, <http://dx.doi.org/10.1103/PhysRevB.75.245402>.
- [15] F. Banhart, J.X. Li, A.V. Krasheninnikov, Carbon nanotubes under electron irradiation: stability of the tubes and their action as pipes for atom transport, *Phys. Rev. B* 71 (2005) 241408, <http://dx.doi.org/10.1103/PhysRevB.71.241408>.
- [16] A.V. Krasheninnikov, F. Banhart, J.X. Li, A.S. Foster, R.M. Nieminen, Stability of carbon nanotubes under electron irradiation: role of tube diameter and chirality, *Phys. Rev. B* 72 (2005) 125428, <http://dx.doi.org/10.1103/PhysRevB.72.125428>.
- [17] A. Santana, A. Zobelli, J. Kotakoski, A. Chuvilin, E. Bichoutskaia, Inclusion of radiation damage dynamics in high-resolution transmission electron microscopy image simulations: the example of graphene, *Phys. Rev. B* 87 (2013) 094110, <http://dx.doi.org/10.1103/PhysRevB.87.094110>.
- [18] S.T. Skowron, I.V. Lebedeva, A.M. Popov, E. Bichoutskaia, Approaches to modelling irradiation-induced processes in transmission electron microscopy, *Nanoscale* 5 (2013) 6677–6692, <http://dx.doi.org/10.1039/c3nr02130k>.
- [19] A.J. Stone, D.J. Wales, Theoretical studies of icosahedral C₆₀ and some related species, *Chem. Phys. Lett.* 128 (1986) 501–503, [http://dx.doi.org/10.1016/0009-2614\(86\)80661-3](http://dx.doi.org/10.1016/0009-2614(86)80661-3).
- [20] J. Kotakoski, J.C. Meyer, S. Kurasch, D. Santos-Cottin, U. Kaiser, A.V. Krasheninnikov, Stone-Wales-type transformations in carbon nanostructures driven by electron irradiation, *Phys. Rev. B* 83 (2011) 245420, <http://dx.doi.org/10.1103/PhysRevB.83.245420>.
- [21] Z. Wang, Y.G. Zhou, J. Bang, M.P. Prange, S.B. Zhang, F. Gao, Modification of defect structures in graphene by electron irradiation: an ab initio molecular dynamics simulation, *J. Phys. Chem. C* 116 (2012) 16070–16079, <http://dx.doi.org/10.1021/jp303905u>.
- [22] J. Ma, D. Alf, A. Michaelides, E. Wang, Stone-Wales defects in graphene and other planar sp²-bonded materials, *Phys. Rev. B* 80 (2009) 033407, <http://dx.doi.org/10.1103/PhysRevB.80.033407>.
- [23] K. Jin, H.Y. Xiao, Y. Zhang, W.J. Weber, Effects of boron-nitride substrates on Stone-Wales defect formation in graphene: an ab initio molecular dynamics study, *Appl. Phys. Lett.* 104 (2014) 203106, <http://dx.doi.org/10.1063/1.4879258>.
- [24] W.A. McKinley, H. Feshbach, The coulomb scattering of relativistic electrons by nuclei, *Phys. Rev.* 74 (1948) 1759–1763, <http://dx.doi.org/10.1103/PhysRev.74.1759>.
- [25] C. Ewels, M. Heggge, P. Briddon, Adatoms and nanoengineering of carbon, *Chem. Phys. Lett.* 351 (2002) 178–182, [http://dx.doi.org/10.1016/S0009-2614\(01\)01371-9](http://dx.doi.org/10.1016/S0009-2614(01)01371-9).
- [26] C. Wang, Y. Ding, Catalytically healing the Stone–Wales defects in graphene by carbon adatoms, *J. Mater. Chem. A* 1 (2013) 1885–1891, <http://dx.doi.org/10.1039/C2TA00736C>.
- [27] A.I. Podlivaev, L.A. Openov, Out-of-plane path of the Stone–Wales transformation in graphene, *Phys. Lett. A* 379 (2015) 1757–1761, <http://dx.doi.org/10.1016/j.physleta.2015.04.010>.
- [28] J. Zubeltzu, A. Chuvilin, F. Corsetti, A. Zurutuza, E. Artacho, Knock-on damage in bilayer graphene: indications for a catalytic pathway, *Phys. Rev. B* 88 (2013) 245407, <http://dx.doi.org/10.1103/PhysRevB.88.245407>.
- [29] R.F. Egerton, P. Li, M. Malac, Radiation damage in the TEM and SEM, *Micron* 35 (2004) 399–409, <http://dx.doi.org/10.1016/j.micron.2004.02.003>.
- [30] A.W. Robertson, C.S. Allen, Y.A. Wu, K. He, J. Olivier, J. Neethling, et al., Spatial control of defect creation in graphene at the nanoscale, *Nat. Commun.* 3 (2012) 1144, <http://dx.doi.org/10.1038/ncomms2141>.
- [31] S. Gilbertson, G.L. Dakovski, T. Durakiewicz, J.-X. Zhu, K.M. Dani, A.D. Mohite, et al., Tracing ultrafast separation and coalescence of carrier distributions in graphene with time-resolved photoemission, *J. Phys. Chem. Lett.* 3 (2012) 64–68, <http://dx.doi.org/10.1021/jz2014067>.
- [32] P.A. George, J. Strait, J. Dawlaty, S. Shivaraman, M. Chandrashekar, F. Rana, et al., Spectroscopy of the carrier relaxation epitaxial graphene, *Nano Lett.* 8 (2008) 17–20, <http://dx.doi.org/10.1021/nl8019399>.
- [33] J.H. Strait, H. Wang, S. Shivaraman, V. Shields, M. Spencer, F. Rana, Very slow cooling dynamics of photoexcited carriers in graphene observed by optical-pump terahertz-probe spectroscopy, *Nano Lett.* 11 (2011) 4902–4906, <http://dx.doi.org/10.1021/nl202800h>.
- [34] K. Yamazaki, N. Niitsu, K. Nakamura, M. Kanno, H. Kono, Electronic excited state paths of stone–wales rearrangement in pyrene: roles of conical intersections, *J. Phys. Chem. A* 116 (2012) 11441–11450, <http://dx.doi.org/10.1021/jp306894x>.
- [35] F. Valencia, A.H. Romero, H.O. Jeschke, M.E. Garcia, Large-amplitude coherent phonons and inverse Stone-Wales transitions in graphitic systems with defects interacting with ultrashort laser pulses, *Phys. Rev. B* 74 (2006) 075409, <http://dx.doi.org/10.1103/PhysRevB.74.075409>.